energies

MDPI

Article

An Improved Comprehensive Model of Pyrolysis of Large Coal Particles to Predict Temperature Variation and Volatile Component Yields

Wenning Zhou [1,2], Hailong Huo [1], Qinye Li [1], Ruifeng Dou [1,2] and Xunliang Liu [1,2,*]

[1] School of Energy and Environmental Engineering, University of Science and Technology Beijing, Beijing 100083, China; wenningzhou@ustb.edu.cn (W.Z.); B20180072@ustb.edu.cn (H.H.); qinye.li@foxmail.com (Q.L.); douruifeng@ustb.edu.cn (R.D.)

[2] Beijing Key Laboratory of Energy Saving and Emission Reduction for Metallurgical Industry, University of Science and Technology Beijing, Beijing 100083, China

* Correspondence: liuxl@me.ustb.edu.cn; Tel.: +86-10-62332741

Received: 21 January 2019; Accepted: 26 February 2019; Published: 7 March 2019

Abstract: In this work, an improved comprehensive model was developed for large coal particles to predict temperature variation and volatile component yields. The kinetics model of volatile component yields, where the volatile matters were assumed to comprise nine species, was combined with heat transfer model. The interaction between volatile yield and heat transfer during pyrolysis of large Maltby coal particles was investigated. An apparent temperature difference has been observed between the surface and core of particles at the initial heating stage. The non-uniform temperature distribution inside coal particles causes non-simultaneous volatile yields release from the surface and core area. The volatile release occurs after the coal temperature rises higher than 350 °C, and its yield steeply increases within the temperature range of 450–520 °C. The peak of volatile release rate corresponds to about 485 °C due to the rapid release of tar and H_2O. The tar is almost completely released at around 550 °C. With the increasing particle size, the difference in temperature and volatile yield between the surface and core increases at the end of heating. The results are expected to provide insights into the interaction between heat transfer and volatile yields during pyrolysis of large coal particles.

Keywords: coal pyrolysis; large coal particles; temperature variation; volatile yield; numerical model

1. Introduction

Coal, one of the primary fossil fuel sources, plays an important role in China, owing to the abundant reserves and its competitively low price compared to natural gas and oil [1]. Direct combustion as a main manner of the utilization of coal, which suffers a high energy penalty for carbon capture and a low energy efficiency [2], requires further improvement. Recently, pulverized coal has been widely used in steel and power plants for improving the burnout of coal, although this technology suffers from separation, crushing, grinding from the raw coal, and pipe blockage issues during the transportation of the pulverized coal [3–7]. Moreover, the need for reduced greenhouse gas emissions has spurred the development of clean coal technology, such as chemical looping combustion (CLC) [8], integrated gasification combined cycle (IGCC) [9], multi-stage coal gasification (MSCG) [10], and so on. These innovative technologies based on the pyrolysis and gasification of coal have been applied in the manufacturing industry. However, pyrolysis, or devolatilization, as the primary process during coal gasification and combustion, plays a key role in determining the gaseous production and carbon structure, which causes an inevitable effect on subsequent processes [11,12]. Li et al. [13] reported the transformation of aggregate structure for low-rank coal by in-situ X-ray diffraction (XRD)

and thermogravimetric analysis-mass spectrometry (TG-MS). They found that the changes of structure parameters were associated with the release characteristics of gaseous products. Nassini et al. [14] showed that the layer structure was observed clearly in high pyrolysis temperature, compared with parental coal, in which the structure seems more disordered. Wen et al. [15] claimed that the decrease in specific capacity was related to the evolution of volatile matter. Lee et al. [16] examined the pore structure variation of coal char during pyrolysis and concluded the higher surface area and better dispersion of ash phase leads to a higher combustion reactivity of the Shievee Ovoo coal (SOC) char. More recently, Bhoi et al. [17] and Gao et al. [18] adopted ReaxFF molecular dynamics simulations to investigate coal pyrolysis at a microscopic view. Meanwhile, the pyrolysis, as part of the coal conversion technology, can extract high-value parts in coal to the gaseous fuel, liquids, and the coke. Therefore, it is essential to comprehensively understand the behaviors of pyrolysis.

A few models have been proposed for simulating the pyrolysis of large coal particles, with a particular focus on heat transfer processes coupled with the devolatilization kinetics. Agarwal et al. [19] studied extensively on devolatilization models for coal combustion processes. Fu et al. [20] developed a general devolatilization model for large coal particles, and they concluded that the kinetics parameters of coal only depended on the final temperature of coal, rather than the coal type. This model was later employed by Wan et al. [21] and the devolatilization characteristic of coal, biomass, and coal–biomass blends were obtained. However, these models mentioned above usually assumed the intraparticle heat transfer to be the rate-controlling mechanism without considering the effect of mass transfer.

Researchers have made a lot of effects on the kinetic numerical model of coal pyrolysis. A single-equation kinetic model was developed by Badzioch et al. [22], and then a two-parallel reaction kinetic model was put forward by Conesa et al. [23]. More recently, Samuele et al. [24] described coal devolatilization with a multi-step kinetic model, which refers to about 30 reactions and lumped species. Chern and Hayhurst [25,26] studied the pyrolysis of large particle coal and small granular coal with an improved nuclear condensation reaction model and first order reaction model, respectively. In addition, some sophisticated models, such as the functional group-depolymerization vaporization crosslinking (FG-DVC) model [27], the chemical percolation devolatilization (CPD) model [28,29] and the distributed activation energy model (DAEM) [30,31] were proposed to describe the precipitation of gas products and the formation of tar. For both the FG-DVC model and the CPD model, the relationship between coal category and model parameters is difficult to determine. In contrast to the FG-DVC model and the CPD model, the DAEM model is relatively simpler, and it is also commonly used to predict the pyrolysis behavior of large coal particles [32]. The DAEM model assumes that the pyrolysis is a combination of a series of parallel chemical reactions, and the activation energy of the reaction is expressed by the Gauss distribution function. The relevant experimental data provided by Solomon et al. [33] and Sadhukhane et al. [7,34] showed that this model is in good accordance with the practical process.

Previous studies [20,21,35] have accurately predicted the temperature distribution and volatile matter release during coal pyrolysis, with the particles size ranging from 3 mm to 16 mm. In respect to large particle sizes, e.g, more than 20 mm, which can be accepted by pyrolysis or gasification in the fixed/moving bed [36] and Lurgi–Spuelgas (L–S) gasifier, they are still under investigation. Wu et al. [37,38] have reported the rotary hearth furnace used in the pyrolysis technology with the particles sized between 10 mm and 100 mm. Although much work has been carried out on coal pyrolysis behaviors, so far there are only a few studies focusing the interaction between heat transfer and volatile yield during pyrolysis of large coal particles. For large coal particles, heat transfer is crucial to the coal pyrolysis. Due to the large particle size and low thermal conductivity of coal, a larger temperature gradient exists inside the particle, and heat conduction is the limiting factor for coal pyrolysis [26]. In our previous studies, we have developed a comprehensive model for coal pyrolysis coupled with heat transfer inside the particle, considering the heat effect of pyrolysis reaction and convective heat transfer due to volatile matters release [39,40]. However, the volatile matters were regarded as a substance for simplification. The composition of volatile matter is complicated, which is

dependent on the original coal sample, heating rate, and final decomposition temperature. In order to describe the kinetics of volatile components release, Merrick [41] proposed a model that included a system of parallel first-order reactions, where the composition of the volatile matter was defined in terms of the following nine species: CH_4, C_2H_6, CO, CO_2, tar, H_2, H_2O, H_2S, and NH_3. However, Merrick's model omitted the heat transfer inside the coal particles and the model is usually applied to small particles.

The aim of this study is to extend our previous research work [39,40] and develop an improved comprehensive model, combining the kinetics model of volatile composition release and the heat transfer model, and investigate the interaction between volatile yield and heat transfer during pyrolysis of large coal particles in the moving bed. In the improved model, the volatile matters were assumed to be a mixture of nine components. The pyrolysis was simulated for large coal particles, up to 60 mm, during heating for an hour, and the effects of particle size on the heat transfer, as well as volatile component yields, were investigated and discussed.

2. Mathematical Model

2.1. Kinetic Model of Volatilization Analysis

In this model, the pyrolysis products of coal particles were assumed as a mixture of nine species of volatile matters and char. The nine volatile matters include CH_4, C_2H_6, CO, CO_2, tar, H_2, H_2O, H_2S, and NH_3. Therefore, the final yields of the volatile matter species can be obtained by a set of ten simultaneous linear equations. These equations can be written as follows [41]:

$$\sum_{j=0}^{9} A_{ij}\overline{m}_j = b_i \ (i = 1, 2, \ldots, 10) \quad (1)$$

where A_{ij} is a matrix of constants; $\overline{m}_j$ denotes the final yields (as mass fractions of daf coal) of char and volatile matter species; and b_i is a vector of constants.

The kinetics of volatile matter release can be described by a system of parallel first-order reactions:

$$\frac{d\delta_j}{dt} = k\exp(-E/RT)(1-\delta_j) \quad (2)$$

where δ_j is the fraction of yield and final yield of volatile matter species released by time t (%), j = 1, 2, ... , 9; k is the frequency factor (1.3×10^{13} s^{-1}); E denotes the activation energy (J·kmol^{-1}); R is the gas constant (8314.4 J·kmol^{-1}) and T represents the temperature (K).

The activation energy distribution corresponds to the Rosin–Rammler function, which can be expressed as:

$$F_j(E) = \exp[-(\frac{E-E_{0j}}{\gamma_j})^{\beta_j}] \ (j = 1, 2, \ldots, 9) \quad (3)$$

In general, the parameters E_{0j}, β_j, and γ_j vary both with the species and with coal rank. γ_j is determined by $\gamma_j = \gamma_{1j} - \gamma_{2j} \ln p$. The adopted parameter values in the model are listed in Table 1 [41].

Table 1. Parameters and values in the model. Reproduced from [41], Elsevier: 1983.

Parameter	CH_4	C_2H_6	CO	CO_2	Tar	H_2	H_2O	NH_3	H_2S
E_0/(MJ·kmol^{-1})	183	183	183	183	183	183	183	183	183
β	2	4	4	4	8	4	8	4	4
γ_1/(MJ·kmol^{-1})	110	61	93	78	23.6	16.2	23.6	106	114
γ_2/(MJ·kmol^{-1})	0	0	0	0	17.6	0	17.6	0	0

For the volatile matter species, except char, the cumulative amount m_j (expressed as a fraction of the daf coal) released at time t was given by:

$$m_j(t) = \overline{m}_j \int_0^1 \delta(t,E)\mathrm{d}F_j(E) = -\overline{m}_j \int_{E_0}^{\infty} \delta(t,E)F'_j(E)\mathrm{d}E \ (j = 1, 2, \ldots, 9) \quad (4)$$

The mass of char remaining at time t can be determined by an overall mass balance:

$$m_0(t) = 1 - \sum_{j=1}^{9} m_j(t) \quad (5)$$

2.2. Heat Transfer Model

In this model, the heat conduction inside the coal particles can be described by the following equation [34]:

$$\frac{\partial(\rho c_p T)}{\partial t} = \frac{1}{r^2}\frac{\partial}{\partial r}(\lambda r^2 \frac{\partial T}{\partial r}) + S \quad (6)$$

where ρ is the density of coal; c_p is the specific heat; λ is the thermal conductivity of coal; S is the source term. The source term includes the endothermic effect of coal pyrolysis and convection heat transfer during the escape of volatile matter [40], which can be depicted as:

$$S = \sum_{j=1}^{9} \rho^0 \Delta H \frac{\mathrm{d}m_j}{\mathrm{d}t} + \frac{Qc_{pv}}{4\pi r^2}\frac{\partial T}{\partial r} \quad (7)$$

where ρ^0 is initial coal density; $\triangle H$ is the pyrolysis reaction heat in unit mass; Q is the mass flow rate of volatile matter release; c_{pv} is the specific heat of volatile matter. Mass flow rate at the place r can be written as:

$$Q = \int_0^r 4\pi r'^2 \rho^0 \sum_{j=1}^{9} \frac{\mathrm{d}m_j}{\mathrm{d}t}\mathrm{d}r' \quad (8)$$

The boundary conditions were given by:

$$\text{Coal center} \ -\lambda \left.\frac{\partial T}{\partial r}\right|_{r=0} = 0 \quad (9)$$

$$\text{Coal surface} \ -\lambda \left.\frac{\partial T}{\partial r}\right|_{r=R} = h(T_g - T_R) + \varepsilon_S \sigma (T_g^4 - T_R^4) \quad (10)$$

where T_g and T_R are the temperature of ambient gas and particle surface, respectively; ε_S is the emissivity of coal; h is the coefficient of external convective heat transfer which is obtained from the calculation of Nu number:

$$Nu = 2.0 + 0.667\mathrm{Re}^{\frac{1}{2}}\mathrm{Pr}^{\frac{1}{3}} \quad (11)$$

The parameters used in the numerical model are shown in Table 2.

Table 2. Parameters used in the model.

Parameter	Value or Equation	Reference
$\rho^{\,0}$ (kg·m^{-3})	850	[42]
λ (J·kg^{-1}·K^{-1})	$\begin{cases} \lambda = 0.23 & T \le 623\text{K} \\ \lambda = 0.23 + 2.24 \times 10^{-5}(T-673)^{1.8} & T > 623\text{K} \end{cases}$	[39,40,43]
c_p (W·m^{-1}·K^{-1})	$\begin{cases} c_p = 1254 & T \le 673\text{K} \\ c_p = 1254 - 1.75(T-623) & T > 673\text{K} \end{cases}$	[39,40,43]
ΔH (kJ·mol^{-1})	−300	[39,40,43]
T_g (°C)	750	-
ε_S	0.9	[20]

2.3. Model Parameters and Final Yields

In the present study, Maltby coal was adopted in the simulation cases. According to the literature [41], the proximate analyses of Maltby coal, tar, and char (daf mass fraction basis) are listed in Table 3. The calculated final yields are given in Table 4.

Table 3. Proximate analyses of coal, tar, and coke (wt % daf basis). Reproduced from [41], Elsevier: 1983.

	C	H	O	N	S	Volatile Matter
Maltby	83.8	5.3	7.1	1.8	2.0	36.3
Tar	85	8.2	4.9	0.9	1.0	-
Char	98	0.2	0.2	1.0	0.6	-

Table 4. The final yields of volatile matter (wt % daf basis).

Product	Final Yield	Product	Final Yield
Char	67.13	Tar	12.49
CH_4	6.94	H_2	1.33
C_2H_6	1.17	H_2O	4.82
CO	2.27	NH_3	1.23
CO_2	1.07	H_2S	1.56

The finite volume method (FVM) was used to discretize heat conduction equation (Equation (6)). The discrete algebraic equations were solved by the tridiagonal matrix algorithm (TDMA). Equation (4) was solved by the trapezoidal rule. The detailed formulation for the double integral over both time and activation energy can be found in our previous work [39,40]. As the thermal effect of pyrolysis and convective heat transfer of volatile matters (Equations (7) and (8)) depends on the volatile release rate, the equations should be coupled and solved iteratively.

The numerical program code was developed by using C# language based on the Microsoft NET Framework. The particles were divided into 100 parts with equal distance along the radial direction. In each time step, Equations (4) and (6) were calculated six times. The solution scheme requires about 300 s on the Intel®Core™ i5-3470 (3.20 GHz) type of personal computer, with the integral time steps of 3600 and activation energy increments of 100, respectively.

3. Results and Discussion

3.1. Model Verification

The model was first verified by being compared with the experimental data of coal pyrolysis [41]. The model predictions of volatile yields were compared with the experimental results of coal water mixture (CWM) and Maltby coals with a particle diameter of 3 mm at a heating rate of 5 °C/min. The comparison is shown in Figure 1. It was found that the prediction agrees well with the experimental

results for CWM. For Maltby coals, there was a slightly under-predicted volatile yield. The reason for this may be that some parameters used in our model, e.g., the frequency factor in Equation (2), were selected by the previous work [41]. However, the temperature gradient, which was neglected in the previous work, is considered in the present study. Compared with previous studies, an improvement of numerical results has been found and the average relative error with experimental results is around 7.5%. Therefore, the agreements are considered satisfactory with the experimental results. It should also be mentioned that the clarification of the heat transfer model for large coal particles with a diameter of up to 16 mm can be found in our previous study [40].

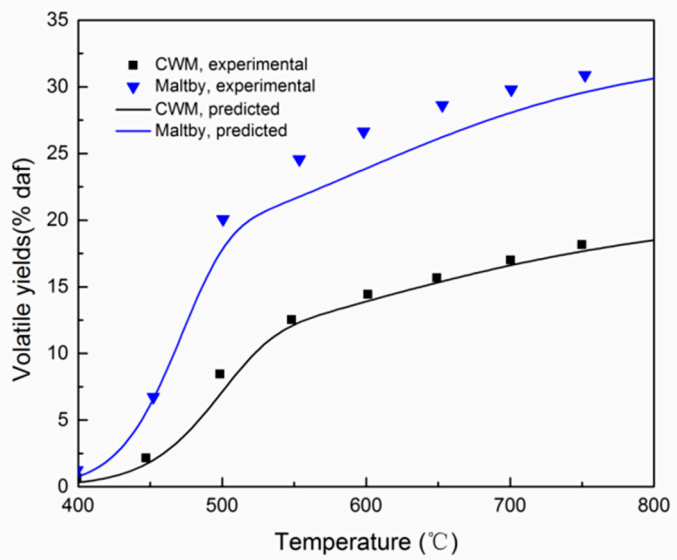

Figure 1. Comparison of prediction and experimental data (Reproduced from [41], Elsevier: 1983) of volatile yields of coal water mixture (CWM) and Maltby coals.

In the following sections, the parameters in the model were set based on Maltby coal and the operating conditions of moving bed. In the moving bed, the coal particles, with the particle diameter ranging from 20 mm to 60 mm, were fed and dropped uniformly. The initial temperature of coal was 150 °C, and the particles were heated by hot inert gas at a rate of 10 °C/min. The gas flows across the packed bed, with the gas temperature decreasing linearly from 750 °C down to 240 °C.

3.2. Temperature Distribution and Volatile Component Yields

To examine the effects of heat transfer inside coal particles on volatile yield, the temperature and volatile yield of different parts inside the particle, including the surface, core, and the middle layer between them (r = 0.5 R) were investigated. The results are plotted in Figure 2. It is observed that the temperature difference between the core and middle layer is less than 10 °C, which indicates that the inner region of the particle has relatively uniform temperature distribution. Therefore, for the sake of simplicity, the core temperature data is applied to represent the temperature at the inner region of the particle in the rest of the content. Due to the low thermal conductivity of coal, a larger temperature difference of up to 67 °C exists between the core and external layer at the initial stage. With the heating processes, the temperature difference gradually decreases down to only 1.7 °C after one hour.

The non-uniform temperature distribution inside coal particles leads to the non-simultaneous, but a similar tendency volatile yields release from the surface and center area of the coal particles, as shown in Figure 2. The increase in volatile matter release can apparently be observed with the temperature of particles. The initial volatile matter yield of surface zone occurs 15 mins later after heating, while that of the center starts up several minutes later than the surface. The volatile yields of both zones increase steeply between 25 and 33 mins, when the corresponding temperatures range from 450 °C to 520 °C. This agrees with our previous model prediction [39,40] and experimental data [31,41,44–46] obtained

by the thermogravimetric analysis. The yields differentiation between the surface and center decreases gradually with the heating process, and finally, both of the volatile yields reached 29%, which accounts for 89% of the final yield.

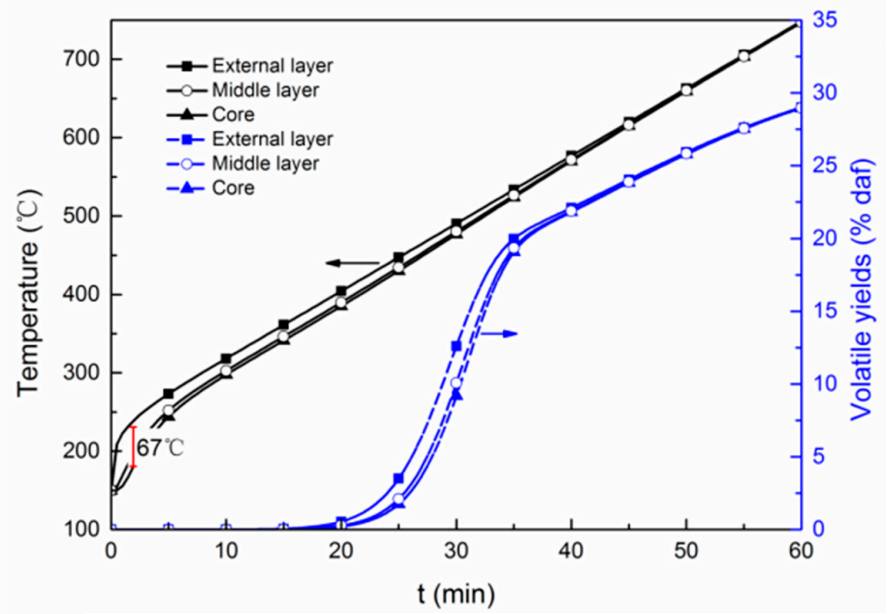

Figure 2. Temperature variation and volatile yield in the different regions of the coal particle with a diameter of 20 mm.

To reveal the relationship between volatile yield and temperature, the volatile yield and its release rate from the coal particle with a diameter of 20 mm are demonstrated against temperature variation in Figure 3. When the temperature is below 350 °C, only a little of the volatile matter is released. After the temperature rises higher than 350 °C, the volatile yield increases gradually and then has a sharp release within the temperature range of 450–520 °C. The peak of release rate corresponds to 485 °C, which is attributed to the fast release of tar and H_2O, as shown in Figure 4. Tar and H_2O have very close temperatures of 476 °C, at which they reach their peak release rates. The two components account for a large proportion of volatile yields, which will be given later.

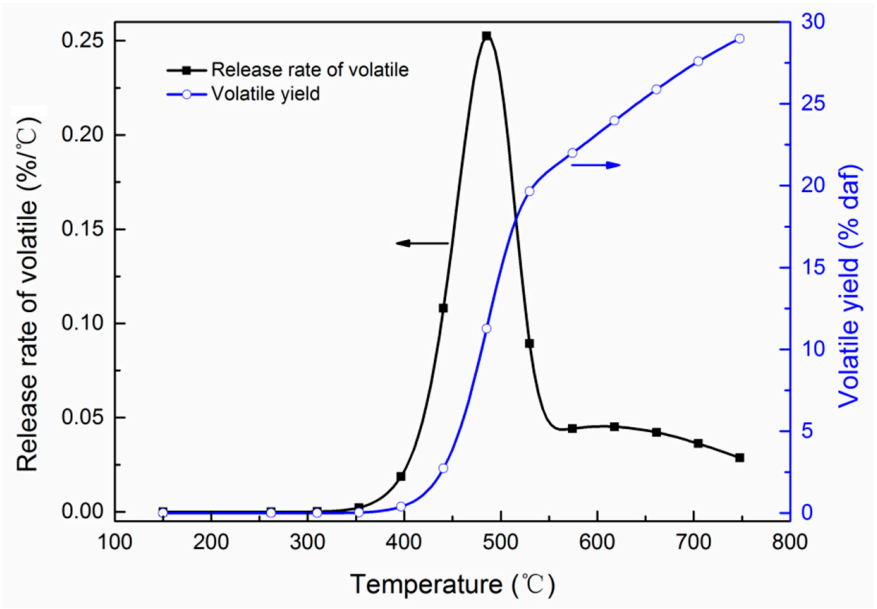

Figure 3. Volatile yield and its release rate from the coal particle as a function of temperature (d = 20 mm).

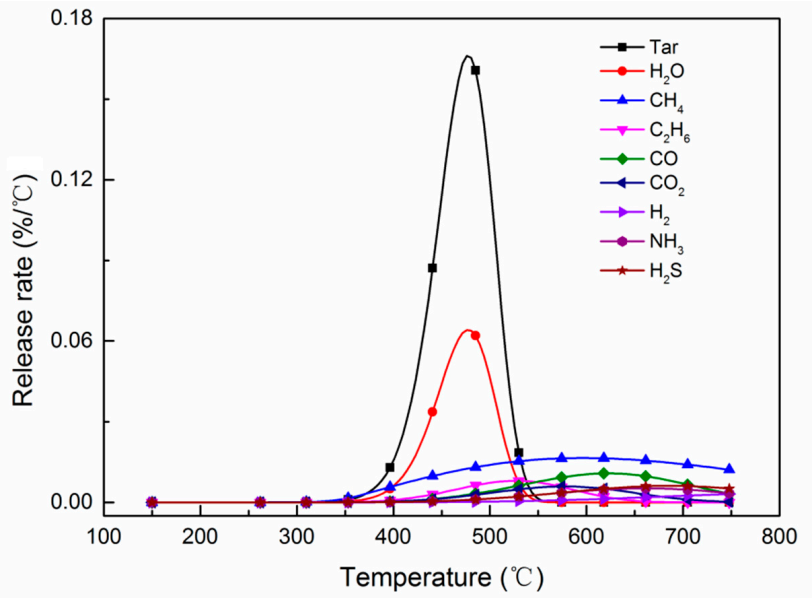

Figure 4. Release rate of tar and H_2O and the tar yield from the coal particle as a function of temperature (d = 20 mm).

In Figure 3, while the temperature is approaching 600 °C, the release rate has another peak with much lower values. This is mainly due to the release of CH_4, which has a maximum rate of 596.1 °C, as displayed in Figure 5. Similar results have also been reported by Zou et al. [47]. They concluded that the product of CH_4 has a wide temperature range, from 331 °C to 907 °C, and its maximum rate occurs around 540 °C. Moreover, these mass loss depicted above are consistent with previous studies [31,47] which can be summarized as three stage: the first stage in the temperature below 300 °C mainly occurs the release of moisture and absorbed gases; the second mass loss in the temperature between 300 °C and 550 °C is the main degradation stage, due primarily to the volatile gases and tars releasing; the last stage from 600 °C to 1000 °C derives from the aromatic ring condensation. The temperatures corresponding to the peak release rates of volatile species are shown in Table 5. The yields of these species are listed in Table 6.

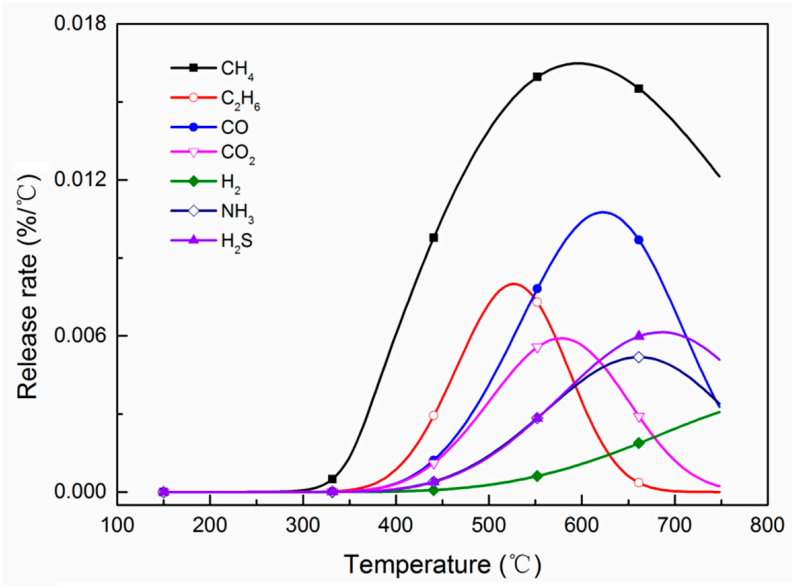

Figure 5. Release rate of other seven volatile components excluding tar and H_2O from the coal particle (d = 20 mm).

Table 5. The temperature corresponding to peak release rate of volatile components.

	CH_4	C_2H_6	CO	CO_2	Tar	H_2	H_2O	NH_3	H_2S
Temp (°C)	596.1	525.5	622.3	578.6	476.2	-	476.2	661.5	687.4

Table 6. Yields of nine components in the volatile matter.

	CH_4	C_2H_6	CO	CO_2	Tar	H_2	H_2O	NH_3	H_2S
Yield (% daf)	5.01	1.17	2.15	1.06	12.49	0.38	4.82	1.03	1.17
Final yield (% daf)	6.94	1.17	2.27	1.07	12.49	1.33	4.82	1.23	1.56
Ratio (%)	72.19	100	94.71	99.07	100	28.57	100	83.74	75.00

In addition, it can be seen from Figures 4 and 5 that the peak rate of tar release (daf mass fraction basis) is about 10 times as much as that of other components, except H_2O. For tar and H_2O, the peak release rate corresponds to the same temperature of 476 °C. When the temperature rises up to 550 °C, the tar yield reaches the final yield of 12.49%. At the end of heating, with the temperature approaching 750 °C, the species of C_2H_6, CO_2, tar, and H_2O were completely released, while others were not, such as CH_4, CO, H_2, H_2S, and NH_3.

3.3. Effect of Particle Size on the Heat Transfer and Volatile Yield

For pyrolysis of large coal particle, internal heat transfer is the limiting factor, due to the low thermal conductivity of the coal. To investigate the effect of particle size on the heat transfer and volatile yield, the pyrolysis was simulated for three kinds of coal particle sizes (with diameters of 20 mm, 40 mm, and 60 mm) under the same heating condition.

Figure 6a,b shows the core temperatures and its rise rate as a function of time during the heating process of particles with different sizes. It was found that, with the increase of coal particle size, it takes more time to raise the core temperature. The core temperature rise rate becomes lower at the initial stage and reaches a peak later. At the end of heating, the core temperature of the particle with a diameter of 60 mm is around 20 °C lower than that with a diameter of 20 mm. As shown in Figure 6b, the second temperature rise rate peak becomes higher and more centralized with the increase in particle size. This is because, in the intraparticle heat transfer, thermal conduction may play a leading role rather than heat convection and radiation. Thus, the temperature gradient becomes more apparent with the increase in particle size, and a thermal inertia or thermal lag occurs in the core temperature–rise history. These results are consistent with the published work [35,40].

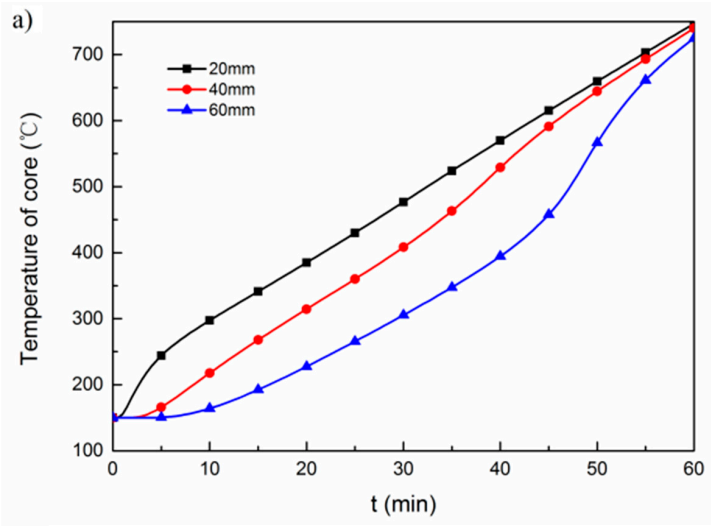

(**a**)

Figure 6. *Cont.*

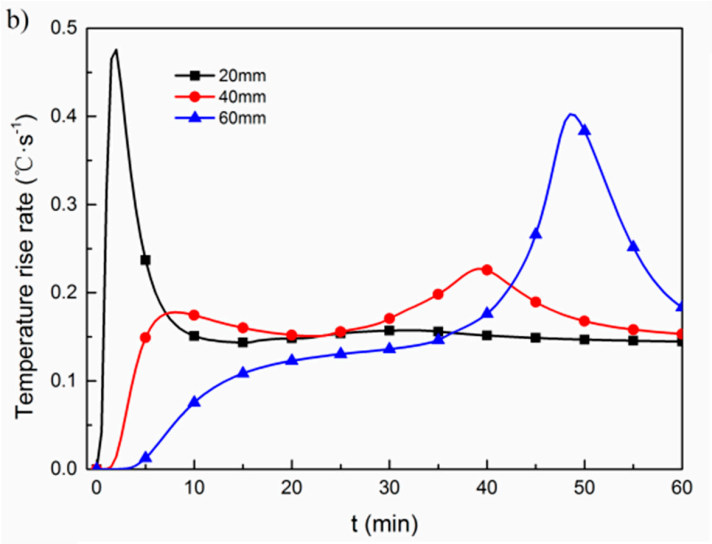

(**b**)

Figure 6. Effect of coal size on the temperature (**a**) and temperature rise rate (**b**) at center of coal particle, 10 °C/min.

Figure 7a,b present the volatile yields and the release rate in the core region of coal particles with different sizes as a function of heating time. It can be seen from the figure that, with the increase of particle size, the initial volatile matter is released much later and achieves a slightly lower yield at the end of heating. Specifically, it takes 15 mins more time to reach the peak volatile release rate for the particles of 60 mm than those of 20 mm. The larger the coal particle is, the greater the release rate peak value it has, as shown in Figure 7b. Compared with Figure 6b, a similar tendency of volatile release rate can be observed due to the difference in the core temperature of the particles. The volatile yield in the core rises more steeply as the coal particle size increases, which is caused by a higher core temperature rise rate within the temperature range of 450–520 °C for a larger particle. The peak rate corresponds to the core temperature of about 485 °C, which is mainly attributed to the release of tar, as displayed in Figure 8.

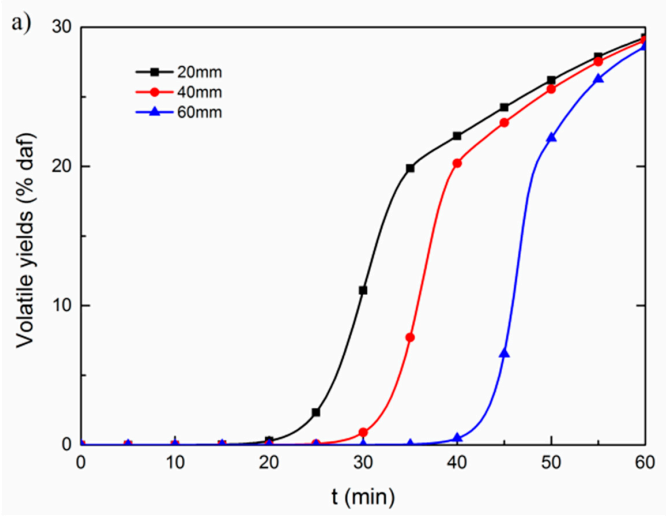

(**a**)

Figure 7. *Cont.*

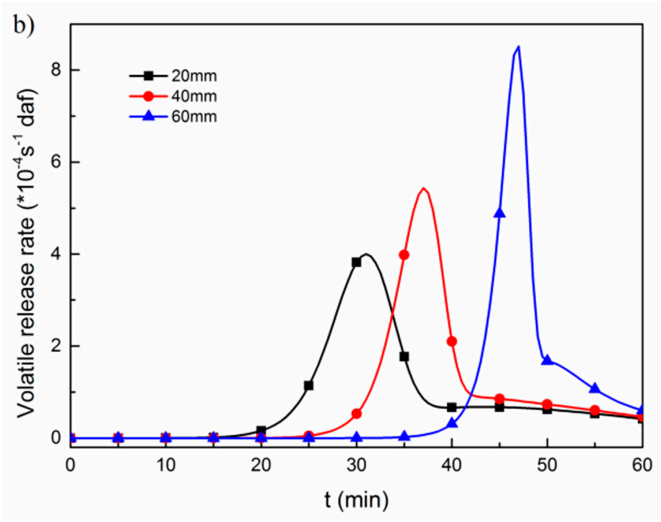

(**b**)

Figure 7. Effect of coal size on the volatile yield (**a**) and its release rate (**b**) at center of coal particle, 10 °C/min.

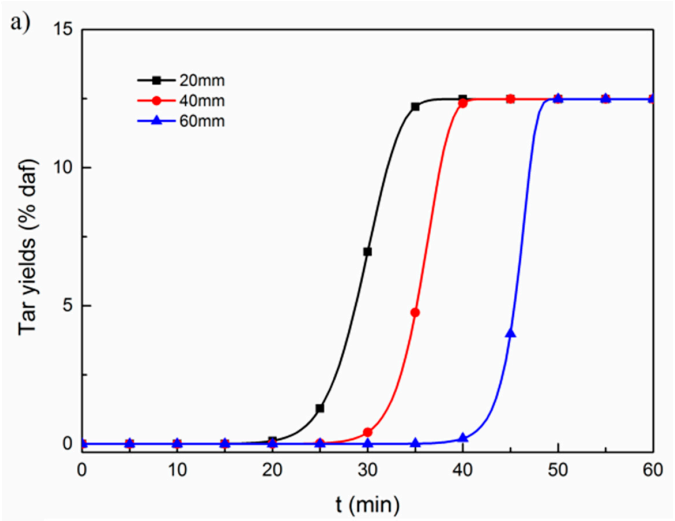

(**a**)

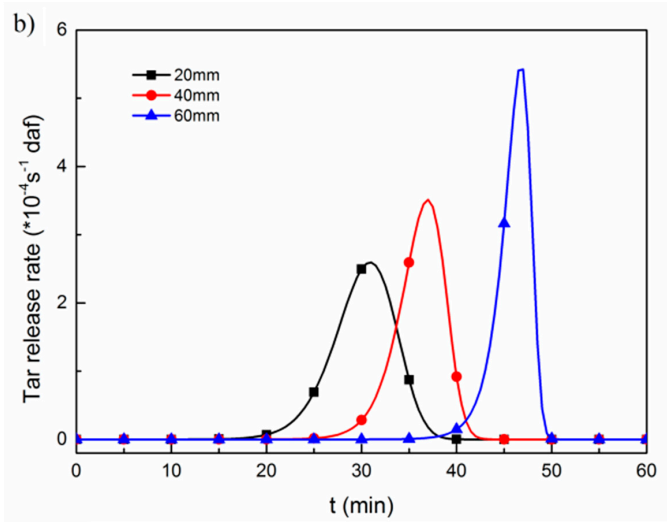

(**b**)

Figure 8. Effect of coal size on the tar yield (**a**) and its release rate (**b**) at center of coal particle, 10 °C/min.

Figure 8a,b display the tar yields and its release rate from different particles as a function of heating time. The difference in the tar release rate from the core can be ascribed to the difference in the core temperature rise rate of coal particles, as shown in Figure 6. It is observed that the tar yields reach their maximums much earlier. This is because the tar and H_2O are completely released when the coal temperature rises up to 550 °C. Other components, such as CH_4, C_2H_6, CO and so on, are sequentially released but with relatively lower rates.

Figure 9 shows the difference of temperature and volatile yield between the external layer and core of three particles with different diameters at the end of heating. After heating for an hour, the temperature difference between the surface and core of the particle with a diameter of 20 mm is around 2 °C, while the volatile yield difference was less than 0.1%. For the particle with a diameter of 60 mm, the temperature difference rose up to 20 °C, and the yield difference was 0.6%. Therefore, to achieve a high volatile yield, the heating time needs to be longer for the larger coal particle. It indicates that the coal feeding rate should be adjusted according to the particle size during the operation of a real L-S retort.

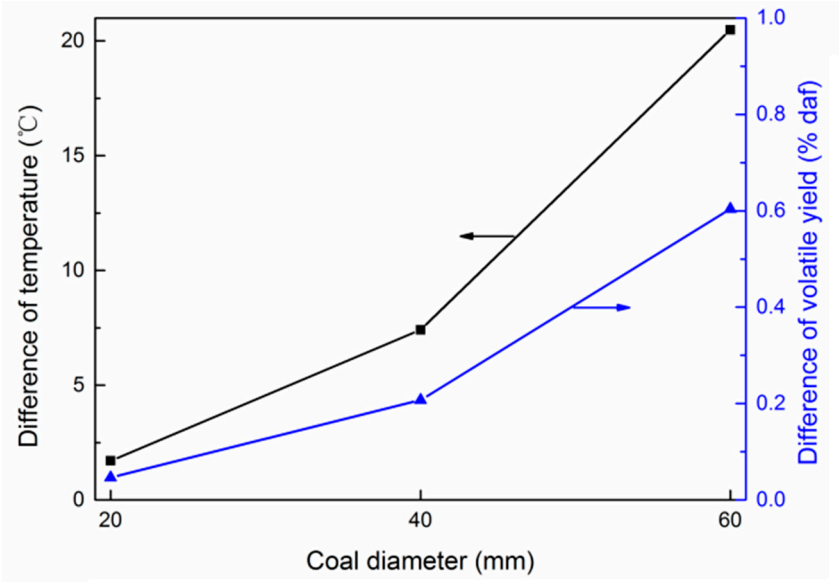

Figure 9. The difference in temperature and volatile yield between the external layer and core of three coal particles with different diameters at the end of heating.

4. Conclusions

In this article, an improved comprehensive model, combining the kinetics model of volatile composition release with the heat transfer model, was developed. In the proposed model, the volatile matters were assumed to comprise nine components. The pyrolysis of large coal particles (Maltby coal particles with diameters ranging from 20 mm to 60 mm) during heating for an hour (temperature linearly increasing from 150 °C up to 750 °C, and heating for an hour at the rate of 10 °C/min) was simulated. The effects of particle size on the pyrolysis and temperature variation were examined. Major conclusions can be drawn as follows.

(1) Due to the low thermal conductivity of coal, a large temperature difference (up to 67 °C for the particle with a diameter of 20 mm) exists between the external layer and core at the initial stage, while the temperature is more uniformly distributed in the inner region near the core.

(2) The volatile yield of the particle increases after the coal temperature rises higher than 350 °C, and has a sharp gain within the temperature range of 450–520 °C. The peak of volatile release rate corresponds to about 485 °C, which is mainly attributed to the fast release of tar and H_2O. When the temperature rises up to 550 °C, the tar is almost completely released approaching the final yield of 12.49%.

(3) With the increase of particle size, more time is needed to raise the inner temperature of the large particle. For the particle with a diameter of 60 mm, the temperature difference between the surface and core increases up to 20 °C at the end of the heating for an hour, and the yield difference is 0.6%. Additionally, the volatile matter is released much later and achieves a slightly lower yield. To achieve a higher volatile yield, the heating time needs to be adjusted to larger coal particles.

Author Contributions: Conceptualization, W.Z. and X.L.; methodology, W.Z., X.L.; software, H.H. and Q.L.; validation, Q.L.; investigation, H.H. and Q.L.; writing—original draft preparation, W.Z., H.H. and Q.L.; writing—review and editing, R.D. and X.L.

Funding: This research was funded by National Key R&D Program of China (Grant No. 2018YFB0605903).

Conflicts of Interest: The authors declare no conflict of interest.

References

1. Bejarano, P.A.; Levendis, Y.A. Single-coal-particle combustion in O_2/N_2 and O_2/CO_2 environments. *Combust. Flame* **2008**, *153*, 270–287. [CrossRef]
2. Adanez, J.; Abad, A.; Garcia-Labiano, F.; Gayan, P.; Luis, F. Progress in chemical-looping combustion and reforming technologies. *Prog. Energy Combust. Sci.* **2012**, *38*, 215–282. [CrossRef]
3. Zhang, Y.-Q.; Liang, P.; Yu, J.; Zhu, J.-L.; Qin, X.-Z. Studies of granular bed filter for dust removal in the process of coal pyrolysis by solid heat carrier. *RSC Adv.* **2017**, *7*, 20266–20272. [CrossRef]
4. Muto, M.; Yuasa, K.; Kurose, R. Numerical simulation of soot formation in pulverized coal combustion with detailed chemical reaction mechanism. *Adv. Powder Technol.* **2018**, *29*, 1119–1127. [CrossRef]
5. Sahu, S.G.; Mukherjee, A.; Kumar, M.; Adak, A.; Sarkar, P.; Biswas, S.; Tiwari, H.; Das, A.; Banerjee, P. Evaluation of combustion behaviour of coal blends for use in pulverized coal injection (PCI). *Appl. Therm. Eng.* **2014**, *73*, 1014–1021. [CrossRef]
6. Rizkiana, J.; Guan, G.; Widayatno, W.B.; Yang, J.; Hao, X.; Matsuoka, K.; Abudula, A. Mg-modified ultra-stable Y type zeolite for the rapid catalytic co-pyrolysis of low-rank coal and biomass. *RSC Adv.* **2016**, *6*, 2096–2105. [CrossRef]
7. Sadhukhan, A.K.; Gupta, P.; Saha, R.K. Modeling and experimental investigations on the pyrolysis of large coal particles. *Energy Fuels* **2011**, *25*, 5573–5583. [CrossRef]
8. Adánez, J.; Abad, A.; Mendiara, T.; Gayán, P.; de Diego, L.; García-Labiano, F. Chemical looping combustion of solid fuels. *Prog. Energy Combust. Sci.* **2017**, *65*, 6–66. [CrossRef]
9. Kobayashi, M.; Akiho, H. Dry syngas purification process for coal gas produced in oxy-fuel type integrated gasification combined cycle power generation with carbon dioxide capturing feature. *J. Environ. Manag.* **2017**, *203*, 925–936. [CrossRef] [PubMed]
10. Chen, Z.; Li, Y.; Lai, D.; Geng, S.; Zhou, Q.; Gao, S.; Xu, G. Coupling coal pyrolysis with char gasification in a multi-stage fluidized bed to co-produce high-quality tar and syngas. *Appl. Energy* **2018**, *215*, 348–355. [CrossRef]
11. Shu, Z.; Wang, J.; Fan, C.; Li, S. Multifluid Modeling of Mixing and Segregation of Binary Gas–Solid Flow in a Downer Reactor for Coal Pyrolysis. *Ind. Eng. Chem. Res.* **2014**, *53*, 9915–9924. [CrossRef]
12. Shu, Z.; Fan, C.; Li, S.; Wang, J. Multifluid Modeling of Coal Pyrolysis in a Downer Reactor. *Ind. Eng. Chem. Res.* **2016**, *55*, 2634–2645. [CrossRef]
13. Li, M.; Zeng, F.; Chang, H.; Xu, B.; Wang, W. Aggregate structure evolution of low-rank coals during pyrolysis by in-situ X-ray diffraction. *Int. J. Coal Geol.* **2013**, *116*, 262–269. [CrossRef]
14. Nassini, D.; Fouga, G.G.; Nassini, H.E.; Bohé, A.E. Effects of pyrolysis conditions on the structure of chars prepared from an Argentine asphaltite. *Fuel* **2016**, *182*, 623–631. [CrossRef]
15. Wen, H.; Lu, J.-H.; Xiao, Y.; Deng, J. Temperature dependence of thermal conductivity, diffusion and specific heat capacity for coal and rocks from coalfield. *Thermochim. Acta* **2015**, *619*, 41–47. [CrossRef]
16. Lee, D.-W.; Bae, J.-S.; Park, S.-J.; Lee, Y.-J.; Hong, J.-C.; Choi, Y.-C. The Pore Structure Variation of Coal Char during Pyrolysis and Its Relationship with Char Combustion Reactivity. *Ind. Eng. Chem. Res.* **2012**, *51*, 13580–13588. [CrossRef]
17. Bhoi, S.; Banerjee, T.; Mohanty, K. Insights on the combustion and pyrolysis behavior of three different ranks of coals using reactive molecular dynamics simulation. *RSC Adv.* **2016**, *6*, 2559–2570. [CrossRef]

18. Gao, M.; Li, X.; Guo, L. Pyrolysis simulations of Fugu coal by large-scale ReaxFF molecular dynamics. *Fuel Process. Technol.* **2018**, *178*, 197–205. [CrossRef]
19. Agarwal, P.; La Nauze, R. Transfer processes local to the coal particle: A review of drying, devolatilization and mass transfer in fluidized bed combustion. *Chem. Eng. Res. Des.* **1989**, *67*, 457–480.
20. Fu, W.; Zhang, Y.; Han, H.; Duan, Y. A study on devolatilization of large coal particles. *Combust. Flame* **1987**, *70*, 253–266.
21. Wan, K.; Wang, Z.; He, Y.; Xia, J.; Zhou, Z.; Zhou, J.; Cen, K. Experimental and modeling study of pyrolysis of coal, biomass and blended coal–biomass particles. *Fuel* **2015**, *139*, 356–364. [CrossRef]
22. Badzioch, S.; Hawksley, P.G. Kinetics of thermal decomposition of pulverized coal particles. *Ind. Eng. Chem. Process Des. Dev.* **1970**, *9*, 521–530. [CrossRef]
23. Conesa, J.A.; Caballero, J.; Marcilla, A.; Font, R. Analysis of different kinetic models in the dynamic pyrolysis of cellulose. *Thermochim. Acta* **1995**, *254*, 175–192. [CrossRef]
24. Sommariva, S.; Maffei, T.; Migliavacca, G.; Faravelli, T.; Ranzi, E. A predictive multi-step kinetic model of coal devolatilization. *Fuel* **2010**, *89*, 318–328. [CrossRef]
25. Chern, J.-S.; Hayhurst, A.N. A model for the devolatilization of a coal particle sufficiently large to be controlled by heat transfer. *Combust. Flame* **2006**, *146*, 553–571. [CrossRef]
26. Chern, J.-S.; Hayhurst, A.N. A simple theoretical analysis of the pyrolysis of an isothermal particle of coal. *Combust. Flame* **2010**, *157*, 925–933. [CrossRef]
27. Solomon, P.R.; Hamblen, D.G.; Carangelo, R.; Serio, M.; Deshpande, G. General model of coal devolatilization. *Energy Fuels* **1988**, *2*, 405–422. [CrossRef]
28. De Girolamo, A.; Tan, V.; Liu, Z.; Zhang, L. Pyrolysis of a lignite briquette–Experimental investigation and 1-dimensional modelling approach. *Fuel* **2018**, *212*, 533–545. [CrossRef]
29. Yang, H.; Li, S.; Fletcher, T.H.; Dong, M.; Zhou, W. Simulation of the Evolution of Pressure in a Lignite Particle during Pyrolysis. *Energy Fuels* **2014**, *28*, 3511–3518. [CrossRef]
30. Vand, V. A theory of the irreversible electrical resistance changes of metallic films evaporated in vacuum. *Proc. Phys. Soc.* **1943**, *55*, 222. [CrossRef]
31. Liu, J.; Ma, J.; Luo, L.; Zhang, H.; Jiang, X. Pyrolysis of superfine pulverized coal. Part 5. Thermogravimetric analysis. *Energy Convers. Manag.* **2017**, *154*, 491–502. [CrossRef]
32. Jiang, X.; Chen, D.; Ma, Z.; Yan, J. Models for the combustion of single solid fuel particles in fluidized beds: A review. *Renew. Sustain. Energy Rev.* **2017**, *68*, 410–431. [CrossRef]
33. Solomon, P.R.; Serio, M.A.; Carangelo, R.M.; Markham, J.R. Very rapid coal pyrolysis. *Fuel* **1986**, *65*, 182–194. [CrossRef]
34. Sadhukhan, A.K.; Gupta, P.; Saha, R.K. Modeling and experimental studies on single particle coal devolatilization and residual char combustion in fluidized bed. *Fuel* **2011**, *90*, 2132–2141. [CrossRef]
35. Wang, J.; Lian, W.; Li, P.; Zhang, Z.; Yang, J.; Hao, X.; Huang, W.; Guan, G. Simulation of pyrolysis in low rank coal particle by using DAEM kinetics model: Reaction behavior and heat transfer. *Fuel* **2017**, *207*, 126–135. [CrossRef]
36. Zeng, X.; Wang, F.; Li, H.; Wang, Y.; Dong, L.; Yu, J.; Xu, G. Pilot verification of a low-tar two-stage coal gasification process with a fluidized bed pyrolyzer and fixed bed gasifier. *Appl. Energy* **2014**, *115*, 9–16. [CrossRef]
37. Pei, P.; Wang, Q.; Wu, D. Application and research on Regenerative High Temperature Air Combustion technology on low-rank coal pyrolysis. *Appl. Energy* **2015**, *156*, 762–766. [CrossRef]
38. Pei, P.; Wang, Q.; Wu, D. Application of regenerative high temperature air combustion technology on low-rank coal pyrolysis. *Energy Procedia* **2015**, *66*, 205–208. [CrossRef]
39. Liu, X.; Pan, G.; Wang, G.; Wen, Z. Mathematical model of lump coal falling in the freeboard zone of the COREX melter gasifier. *Energy Fuels* **2011**, *25*, 5729–5735. [CrossRef]
40. Liu, X.; Wang, G.; Pan, G.; Wen, Z. Numerical analysis of heat transfer and volatile evolution of coal particle. *Fuel* **2013**, *106*, 667–673. [CrossRef]
41. Merrick, D. Mathematical models of the thermal decomposition of coal: 1. The evolution of volatile matter. *Fuel* **1983**, *62*, 534–539. [CrossRef]
42. Merrick, D. Mathematical models of the thermal decomposition of coal: 3. Density, porosity and contraction behaviour. *Fuel* **1983**, *62*, 547–552. [CrossRef]

43. Adesanya, B.A.; Pham, H.N. Mathematical modelling of devolatilization of large coal particles in a convective environment. *Fuel* **1995**, *74*, 896–902. [CrossRef]
44. Song, H.; Liu, G.; Zhang, J.; Wu, J. Pyrolysis characteristics and kinetics of low rank coals by TG-FTIR method. *Fuel Process. Technol.* **2017**, *156*, 454–460. [CrossRef]
45. Zhang, L.; Hower, J.C.; Liu, W.-L. Non-isothermal TG-DSC study on prediction of caking properties of vitrinite-rich concentrates of bituminous coals. *Fuel Process. Technol.* **2017**, *156*, 500–504. [CrossRef]
46. Xie, X.; Zhao, Y.; Qiu, P.; Lin, D.; Qian, J.; Hou, H.; Pei, J. Investigation of the relationship between infrared structure and pyrolysis reactivity of coals with different ranks. *Fuel* **2018**, *216*, 521–530. [CrossRef]
47. Zou, C.; Ma, C.; Zhao, J.; Shi, R.; Li, X. Characterization and non-isothermal kinetics of Shenmu bituminous coal devolatilization by TG-MS. *J. Anal. Appl. Pyrolysis* **2017**, *127*, 309–320. [CrossRef]

© 2019 by the authors. Licensee MDPI, Basel, Switzerland. This article is an open access article distributed under the terms and conditions of the Creative Commons Attribution (CC BY) license (http://creativecommons.org/licenses/by/4.0/).